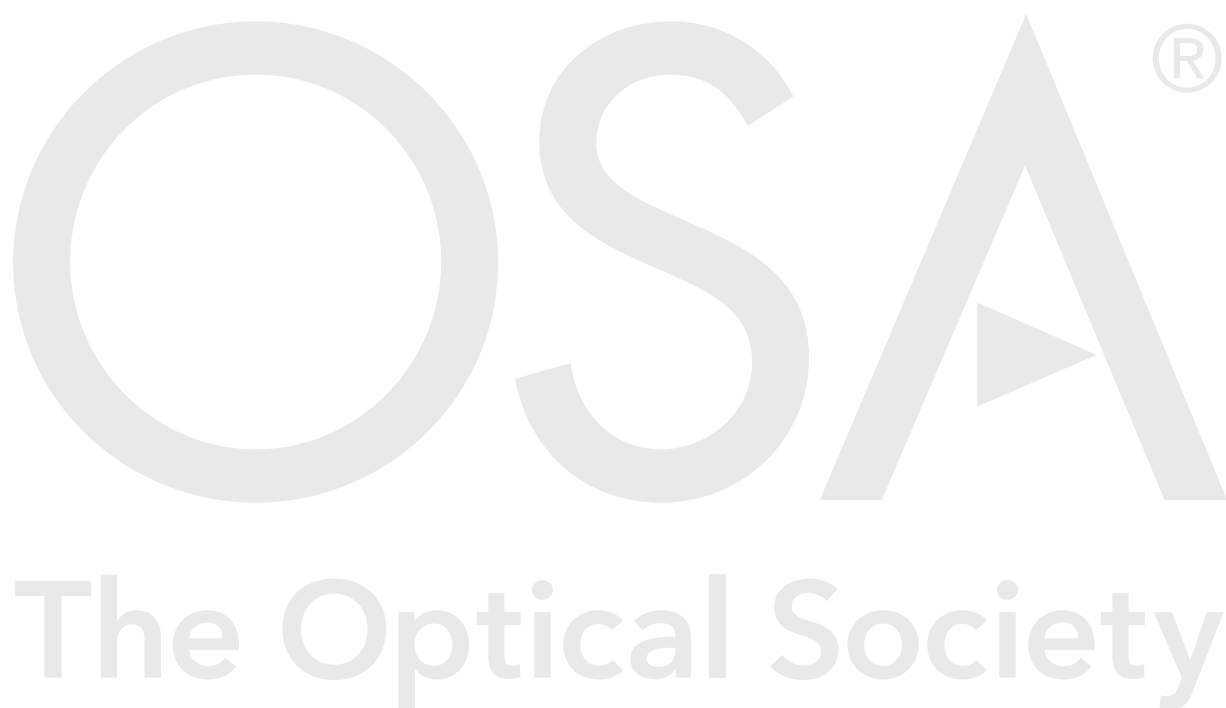


Supplemental document accompanying submission to *Optica*

**Title:** Two-Dimensional Quantum Walk of Correlated Photons

**Authors:** Xianmin Jin, Zhi-Qiang Jiao, Jun Gao, Wen-Hao Zhou, Xiao-Wei Wang, Ruo-Jing Ren, Xiao-Yun Xu, Lu-Feng Qiao, Yao Wang

**Submitted:** 3/22/2021 8:18:09 AM



# Two-Dimensional Quantum Walks of Correlated Photons

## 1. 2D PHOTONIC TRIANGULAR LATTICE FABRICATION

Focusing femtosecond-laser pulses into a borosilicate glass (Eagle XG) sample permanently modifies the material in the focal volume, resulting in a refractive index increase. A second harmonic generation of the femtosecond laser system supplies 290fs pulse at a central wavelength of 513nm with a repetition rate of 1MHz. We feed the laser into a cylindrical lens to reshape the beam into a narrow one and then focus the laser beam by a 50X objective lens (0.55NA) into the 5 cm long substrate to inscribe waveguides array through moving the substrate held on a high-precision air-bearing stage. We use the ABL1500 series air-bearing stages to fabricate the photonic chip, and the error of this stage is less than 50 nm in the whole functional range, which causes slight imperfections corresponding to 15μm, the coupling distance of the chip. An active feedback system locks the fs-laser power. We fix the laser power to 210mW and a constant writing velocity of 15mm/s. This high-precision control system guarantees the homogeneity of the chip, and Fig.2(b) subset shows the final cross-section of the chip. The middle layer waveguides lie in the depth of 170μm below the surface. The injection port distance is 130μm with a bending radius of 30mm. The coupling zone shares the same structure as Fig.1(b), and we choose an evolution length of 11mm. We adiabatically expand the waveguide pitch of 15μm in the coupling zone to match the 3D fanout pitch of 35μm in an adiabatic length of 4mm, as Fig. S1 shows.

## 2. COUPLING STRENGTHS CHARACTERIZATION

We inject a horizontal 780nm laser into the waveguide to characterize a series of coupling strengths shown in Fig. S2. The coupling strength displays an exponential decay along with the separation between two sites. In our experiment, we choose 15μm for the waveguide spacing. The fluctuations of the high-precision air-bearing stage is about 50 nm during the whole functional range of 200mm, which is negligible compared to the coupling distance 15 μm. Thus, technical imperfections cause slight influences during the whole fabrication process. The fluctuations of coupling strength are mainly influenced in the measurement process, which is in a small order in 15 μm. Our high-precision control system guarantees the stability of the fabrication process. The similarity of single-photon evolution patterns between experiments and simulations indicates that the asymmetries and imperfections are negligible.

## 3. CHARACTERIZATIONS OF THE PHOTON SOURCE

We measure the photon source visibility by a Hong-Ou-Mandel interference experiment by continuously tune the relative distance of the correlated photon pair. The dip visibility shows 95.6%±2.45%. The error bars are given by Poisson distributions assumption of the coincidence photon counts. Then we use a balanced fiber beam splitter to separate one arm of the photon pair linked to single-photon detectors and scan the relative distance smoothly to collect the coincidence counts. The coincidence counts show a HOM peak while all the results are displayed in Fig. S3.

## 4. CONTINUOUS QUANTUM WALK ON A CHIP

In a photonic lattice, the mode fields of neighboring single-mode waveguides are overlapped, and light in waveguides can experience quantum tunneling. Photons propagating through evanescently coupled waveguides is defined by the following Hamiltonian[1],

$$H = \sum_{i=1}^N \beta_i a_i^\dagger a_i + \sum_{i \neq j=1}^N C_{i,j} a_i^\dagger a_j. \quad (S1)$$

where  $H$  is equivalent to the adjacency matrix of the connected graph,  $\beta_i$  is the propagation constant of site  $i$ , and the coupling strength between different sites  $i$  and  $j$  is  $C_{i,j} = C_{j,i}$ . In general,

we only consider quantum tunneling that happens between one site and its nearest neighbors. For example, port 0 has 6 possible trajectories.  $a_i^\dagger$  ( $a_i$ ) is the bosonic creation (annihilation) operator for site  $i$ . The propagation dynamics of a single photon is described by Heisenberg equation of motion,  $da^\dagger(z)/dz = -i[a^\dagger, H]/\hbar$ . We replace the evolution time  $t$  by length  $z = ct$ , where  $c$  is the light speed inside waveguide. Since the Hamiltonian is time independent, we can simplify the unitary evolution operator to be  $U = \exp(-iHz)$ . The solution of the equation regarding the operator is  $a_j^\dagger(z) = \sum_{i=1}^N U_{j,i}(z)a_i^\dagger(0)$  by applying unitary operator on the input mode operator  $a_i^\dagger$ . The single-photon evolution distribution is calculated by the average photon number  $n_j = \langle a_j^\dagger a_j \rangle$  in site  $j$ , where the probability of photons in site  $j$  can be calculated by  $|U_{j,i}(z)U_{j,i}^\dagger(z)|$ . Coincidence measurements can be described via quantum correlation function,

$$\Gamma_{i,j}(z) = \langle \psi(0) | a_i^\dagger(z)a_j^\dagger(z)a_j(z)a_i(z) | \psi(0) \rangle. \quad (S2)$$

There are two different ways to realize quantum computation and simulation. One is universal architecture, based on quantum gates, and the other is analog architecture, which focuses on a particular problem and constructs a corresponding Hamiltonian to solve a single task that is hard or intractable in classical regimes. Our system is relatively stable and reconfigurable to implement such kind of tasks. Thus we can adjust the coupling strengths or cite potentials to adapt a variety of quantum tasks. We experimentally fabricate a series of evolution patterns over different evolution lengths of a given Hamiltonian corresponding to different unitary operations. The light density distributions are measured by injecting coherent light into port 0, as Fig. S4 shows.

## 5. VERTICES AND EDGES IN THE ENLARGED GRAPHS

The graph is widely applied in computer science and quantum information physics related to complex networks[2]. In a quantum walk experiment, when involving more than one indistinguishable walker, the quantum interference will exponentially enlarge the newly generated graph[3, 4]. In this part, we introduced how to calculate the vertices and edges in enlarged graphs.

For a given graph  $G$  and  $H$ , it consists of vertices  $V(G) = (1, 2, 3)$ ,  $V(H) = (a, b)$  and edges  $E(G) = [(1, 2), (2, 3)]$ ,  $E(H) = [(a, b)]$  respectively, as Fig.S5 shows. The enlarged graph  $G_E$  is defined by[5],  $G \square H$ . The vertex of  $G_E$  is readily obtained by Cartesian product  $V(G) \times V(H)$ . Edges in  $G_E$  requires that for any two vertices  $u = (u_1, u_2)$  and  $v = (v_1, v_2)$  in  $V(G_E)$ , whenever, either

$$u_1 = v_1 \quad \text{and} \quad (u_2, v_2) \in H \quad (S3)$$

or

$$u_2 = v_2 \quad \text{and} \quad (u_1, v_1) \in G \quad (S4)$$

According to the definition, we can calculate the edges point by point based on the vertices in the enlarged graph  $G_E$ . However, it will cost huge resources. A more efficient method is provided in [6] using adjacency matrix, which is a square matrix representing the connections of a finite graph.

In our case, the elements 0, 1 represent connected or not of two vertices in graphs, respectively. We can get the adjacency matrix of  $G$  and  $K$ ,

$$\begin{pmatrix} 0 & 1 & 0 \\ 1 & 0 & 1 \\ 0 & 1 & 0 \end{pmatrix} \quad (S5)$$

$$\begin{pmatrix} 0 & 1 & 1 \\ 1 & 0 & 1 \\ 1 & 1 & 0 \end{pmatrix} \quad (S6)$$

The edge number in Graph  $G$  and  $K$  equals half of the cumulative sum of adjacency matrix elements. For an enlarged graph, the adjacency matrix is given by,

$$\mathbf{A}_{G_E} = \mathbf{A}_G \otimes \mathbf{I}_H + \mathbf{I}_G \otimes \mathbf{A}_H \quad (S7)$$

where  $\mathbf{A}_{G,H}$  are the adjacency matrices of graph  $G, H$ ;  $\mathbf{I}_{G,H}$  denotes the  $n \times n$  identity matrix and  $n$  is the vertex number of  $G, H$ ;  $\otimes$  means the Kronecker product of matrices. We can get the connections of enlarged graphs in Fig.S5(a) and (b) are 7 and 9, respectively. In our experiment, we got a  $37 \times 37$  adjacency matrix from the triangular lattice. When plugged into Eq.(S7), the number of edges equals 6,660.

## 6. THE COMPLEXITY OF GRAPH

Triangular lattice is one of the fundamental structures of the 2D lattice. In a quantum walk experiment, the quantum interference will exponentially enlarge the newly generated graph when involved more than one indistinguishable walker. For a 1D lattice with two particles, the number of graph dimensions will grow to two. However, a triangular lattice will turn into the 3D graph as Fig.S6(d) shows. The 3D triangular lattice has more edges compared to the 2D square lattice. In this vein, the triangular lattice is more complex than the 1D linear lattice. Moreover, high-dimensional structures can simplify the problem in lower dimensions, such as simulating two-particle dynamics in a 1D lattice using a 2D lattice. In essence, a triangular lattice has more edges than an 1D lattice with the same number of vertices.

The vertices and edges embody the complexity of the graph. It is obvious that the complexity of the graph increase with vertex numbers taking Fig. S5 (a) as an example. Similarly, the complexity of the graph will increase with edge numbers that a single vertex contains. As Fig. S5 shows, the triangular lattice (c) (or enlarged graph (d)) is more complex than (a) (or (b)). The edges will take more possible transitions between different quantum states, especially for database search algorithms. The triangular lattice has six adjacent edges, which allows the largest connectivity number in a scalable 2D lattice. This feature helps us construct complex graph structures with no counterpart in classical regimes with more than one indistinguishable photon. The advantages of the triangular lattice will be more obvious when scaled up. Besides, triangular lattice means a flexible way to generate a variety of 2D lattices to uncover unexplored physics in complex graph conditions, such as square lattice, hexagonal lattice, and Kagome lattice Fig. S6.

## REFERENCES

1. L. E. Estes, T. H. Keil, L. M. Narducci, "Quantum Mechanical description of two coupled harmonic oscillators." *Phys. Rev.* **175**, 286 (1968).
2. J. Biamonte, M. Faccin, M. De Domenico, "Complex networks from classical to quantum." *Commun. Phys.* **2**, 53 (2019).
3. Y. Bromberg, Y. Lahini, R. Morandotti, Y. Silberberg, "Quantum and classical correlations in waveguide lattices." *Phys. Rev. Lett.* **102**, 253904 (2009).
4. A. Peruzzo, M. Lobino, J. C. F. Matthews, N. Matsuda, A. Politi, K. Poulios, X.-Q. Zhou, Y. Lahini, N. Ismail, K. Wörhoff, Y. Bromberg, Y. Silberberg, M. G. Thompson, J. L. O'Brien, "Quantum walks of correlated photons." *Science* **20**, **329**, 1500-1503 (2010).
5. G. Sabidussi, "Graph multiplication." *Math. Zeitschrift*, **72** 446-457 (1960).
6. A. Kaveh, H. Rahami, "A unified method for eigendecomposition of graph products." *Commun. Numer. Meth. Engng.* **21** 377-388 (2005).

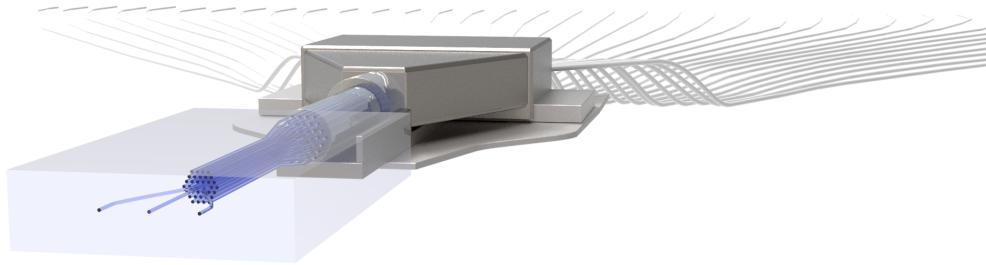


**Fig. S1. Sketch of 3D fanout interface connected to the 2D photonic lattice.** The photonic lattice has three input ports and 37 sites in the coupling zone with  $15\mu\text{m}$  spacing. The coupling zone expands adiabatically to  $35\mu\text{m}$  to match the 3D fanout interface. All fibers are connected to APDs, and MCCM records all coincidence measurements simultaneously.

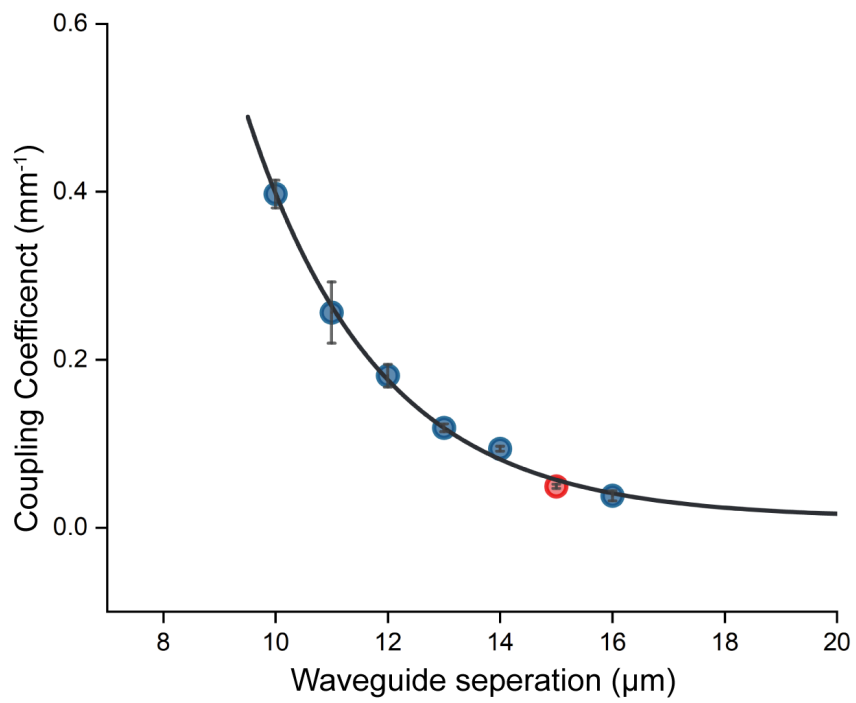


**Fig. S2.** Characterizations of the coupling strengths with different spatial separations. The coupling strength curve displays an exponential decay. In our experiment, the spacing in the coupling zone is chosen as  $15\mu\text{m}$ .

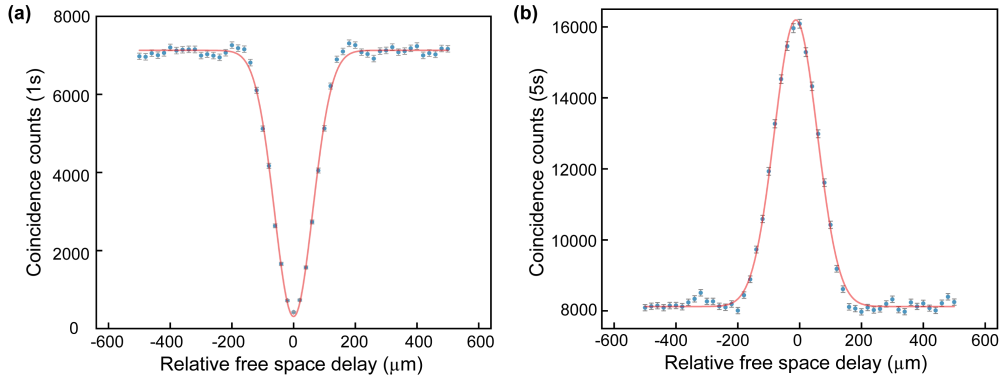


**Fig. S3. HOM interference of the photon source.** (a) The HOM dip of the photon source shows the visibility of  $95.6\% \pm 2.45\%$ . (b) The HOM peak of the photon source shows the visibility of  $98.1\% \pm 0.67\%$ .

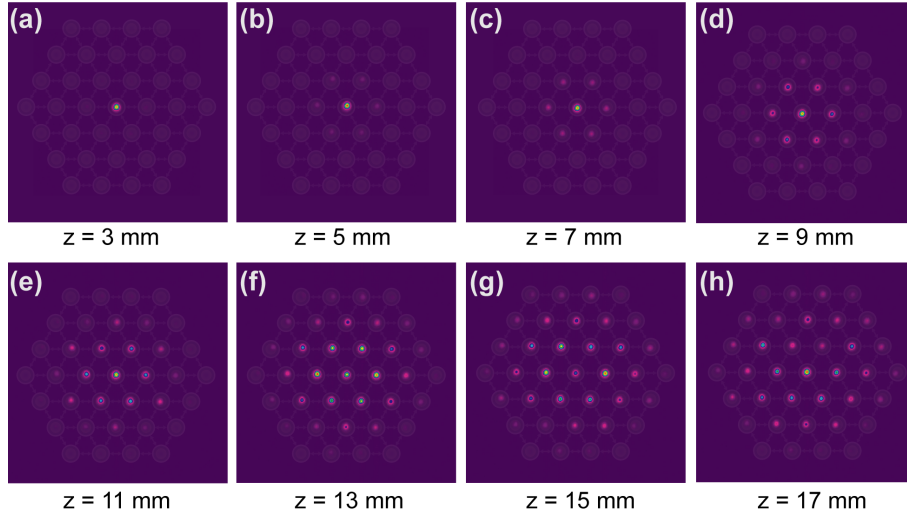


**Fig. S4. Quantum walks patterns of different evolution lengths.** The light density distributions are measured by injecting coherent light into port 0. Evolution lengths are label below the figures from 3 mm to 17 mm with an interval of 2 mm.

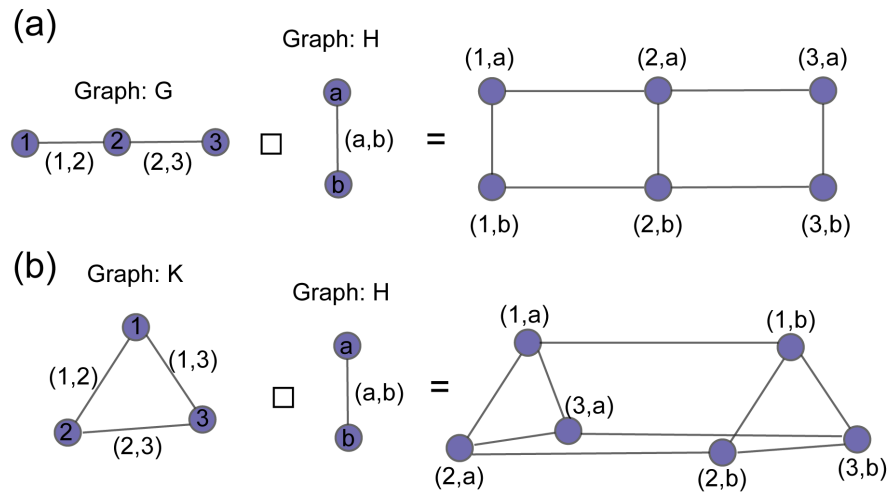


**Fig. S5. Illustration of graph product.** (a) The enlarged graph of  $G$  and  $H$ . (b) The enlarged graph of  $K$  and  $H$ .

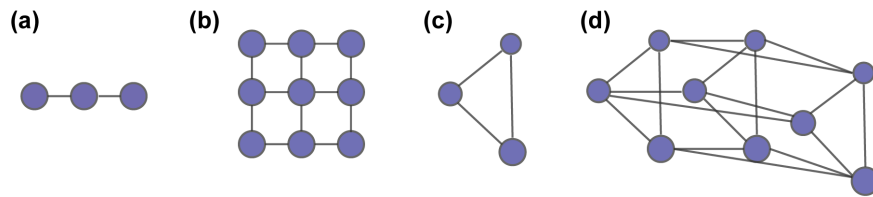


**Fig. S6. Graph dimension with different number of walkers.** (a) and (c) are graph structures with one walker while (b) and (d) are the enlarged graphs of two quantum walkers respectively.

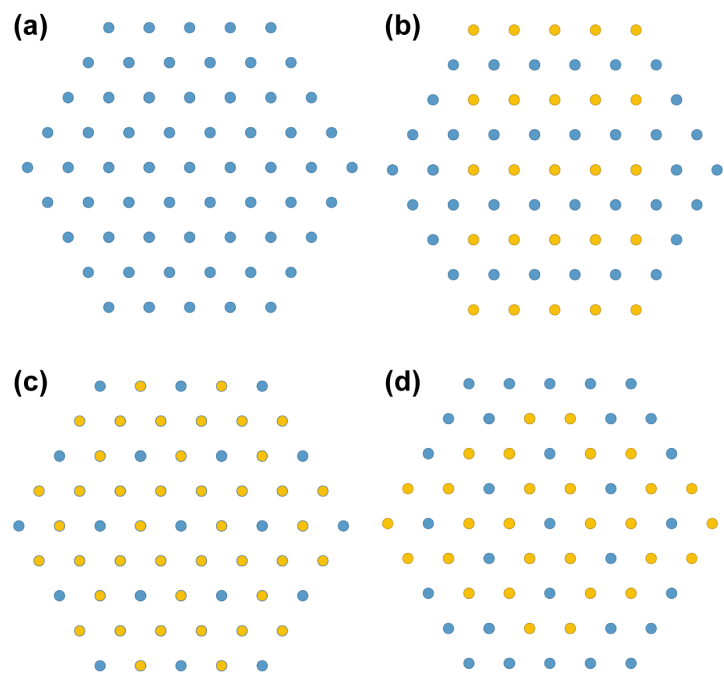


**Fig. S7. 2D Lattice models.** (a) Triangular lattice. (b) Square lattice. (c) Kagome lattice. (d) Hexagonal lattice .